

Cyclotron Resonance of Electrons in Molecular
Afterglows

by

R. V. Jones

and

W. Dobrowolski, W. Kunkel, C. D. Jeffries

Department of Physics

University of California, Berkeley

Note: This report, presented in a **brief** and preliminary way at the 1955 Washington Meeting of the American Physical Society, is abstracted from a part of the Ph.D. thesis of R. V. Jones, submitted in January 1956 to the University of California.

ABSTRACT

Cyclotron Resonance in Molecular Afterglows

A preliminary study of the cyclotron resonances of the free electrons in nitrogen and oxygen afterglows carried out in a paramagnetic resonance spectrometer is described. Since the paramagnetic resonances of the atomic nitrogen and oxygen present in the afterglows as well as the cyclotron resonances of the electrons were observed, estimates of the relative densities are made. Under typical conditions in the nitrogen afterglow these densities are found to be

$$n(N) \cong 4 \times 10^{13} \text{ nitrogen atoms/cc,}$$

$$n(O) \cong 4 \times 10^{12} \text{ oxygen atoms/cc,}$$

$$n(e) \cong 8 \times 10^9 \text{ electrons/cc.}$$

A theoretical discussion of cyclotron power absorption mechanisms is given in terms of a simple Lorentzian picture and from the point of view of the Boltzmann transport theory. This discussion leads to several expressions for the shape function of the power absorption curves and their associated widths. These widths are compared to experimentally determined values under a variety of conditions. Determinations of low energy collision cross sections are made by these comparisons.

CYCLOTRON RESONANCE IN MOLECULAR AFTERGLOWS

A. INTRODUCTION

The resonance absorption of electromagnetic radiation by a system of free electrons under the influence of a magnetic field as the frequency of the radiation approaches the magnetic field's characteristic "cyclotron" frequency is a subject of well established importance. The earliest study of this phenomenon arose in connection with observations of the selective polarization of radio waves reflected from the ionosphere. Since the resonant frequency is a direct measure of the effective mass of the charge carrier, recent observations of cyclotron resonance in semiconductors yield valuable information on the nature of electronic energy surfaces.^{1,2} Several investigators have reported resonance effects in gaseous discharges that can only be explained on the basis of some type of cyclotron process.³⁻⁸ However, the irreproducibility and complexity of breakdown processes involved makes these effects difficult to study.

The long living, pale orange, nitrogen afterglow which persists after an initial excitation of nitrogen gas in a discharge is known to have a rather high density of free electrons ($\approx 10^8$ electrons/cc) associated with it under certain conditions.⁹ It was suggested that the cyclotron resonance of these electrons could be studied in a spectrometer which had been designed and constructed for use in the observation of paramagnetic resonance in gases.* The experiments reported here may be considered as a preliminary survey of the potential utility of applying resonance techniques to the study of such

* R. V. Jones, W. Dobrowolski, W. B. Kunkel, C. D. Jeffries, Bull. Amer. Phys. Soc. 30, 46 (1955).

gas-plasma systems.

Our experiments are distinguished from previously reported work with gaseous cyclotron effects in two essential aspects. Firstly, the steady state nature of the nitrogen afterglow makes possible reasonably controlled and reproducible experimental conditions. Secondly, the experiments are performed in a paramagnetic resonance spectrometer, so it is possible to observe simultaneously the cyclotron resonance of the electrons and the spin resonance of any paramagnetic species present in the afterglow.

The steady state and controllable aspect of the nitrogen afterglow mechanism makes the technique advantageous for the study of the dynamics of the electrons in the plasma. By adjusting the radiofrequency power incident on the afterglow, one may vary the effective temperature of the electrons at will. The shape of the power absorption curve as a function of applied frequency or magnetic field will depend on the nature of the absorption process and the collision cross section of the electrons. If this shape can be interpreted theoretically, then data on the low energy electron cross sections as a function of temperature can be obtained. These measurements would supplement existing static microwave data.¹⁰ We have made preliminary exploratory steps towards this type of analysis.

Since the spin resonance and cyclotron resonance can be observed simultaneously, a comparison of signal heights constitutes a useful method for determining the relative and absolute abundances of electrons and various paramagnetic species present. Beringer working at Yale

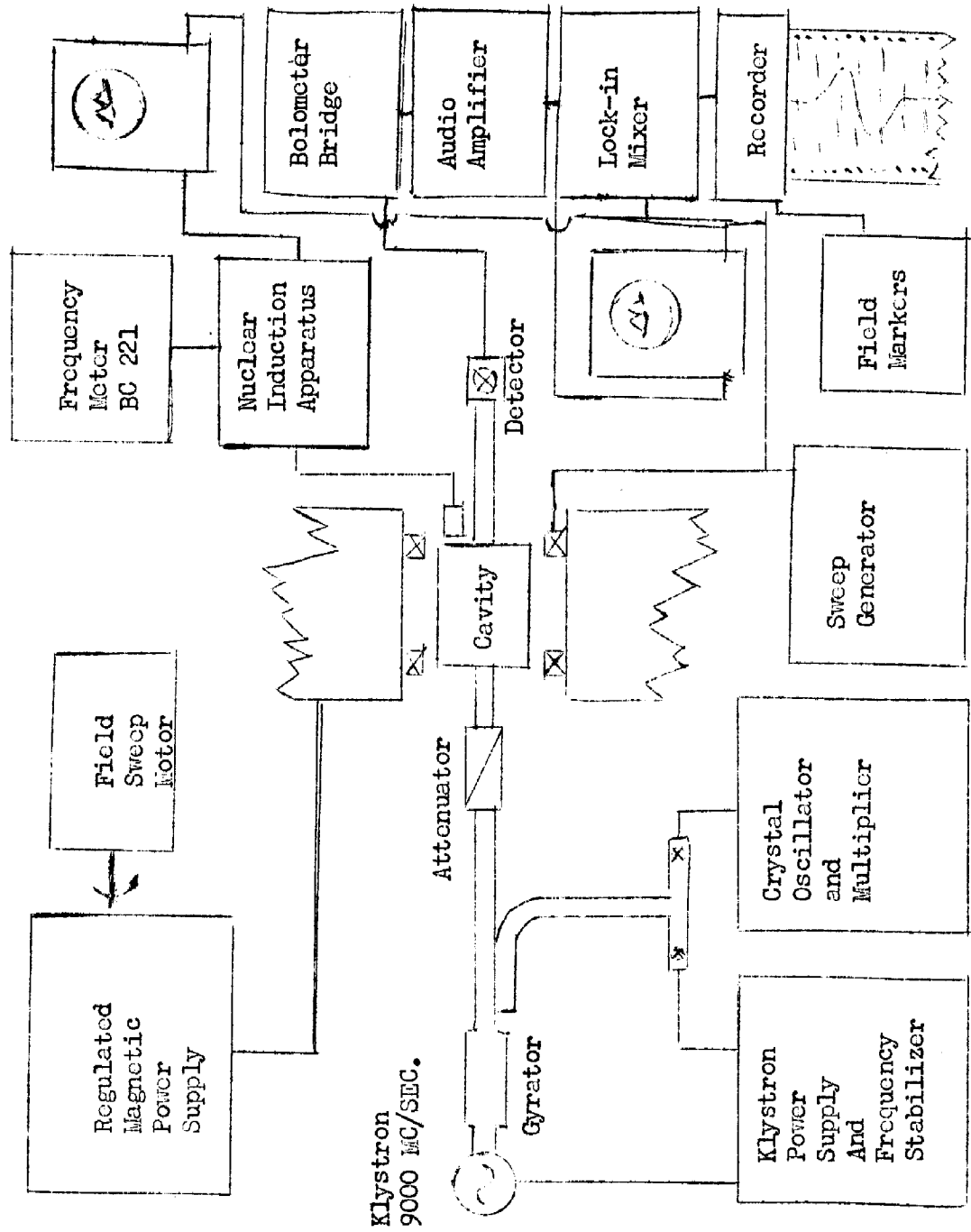
with a similar type of apparatus has reported the observation of resonances in nitrous oxide, nitric oxide, atomic hydrogen, atomic nitrogen, atomic and molecular oxygen.¹¹⁻¹⁶ However, because of the different power absorption mechanism involved in the two types of resonances, at least some simple interpretation of the line shape must be made in order to compare densities. Using the simplest assumptions possible, we have made representative estimates of the abundances involved.

B. EXPERIMENTAL METHODS

GENERAL

The spectrometer used in these experiments was originally designed for the observation of paramagnetic resonances of species in a gaseous state. The important components of the spectrometer and their interrelations are indicated in the block diagram (Figure 1). A section of 15 mm quartz tubing, which comprises part of the gas flow system, passes coaxially through the cylindrical, transmission cavity which is placed between the pole faces of a high impedance electronically regulated magnet. The microwave power is supplied to the cavity by an X-13 Varian reflex klystron, operating at about 9 Kmc/sec. After the output of the klystron has passed through an isolating "Uniline" gyrator, it is sampled by a 12.5 db directional coupler. This sampling activates a frequency stabilizing circuit. The power transmitted through the cavity is detected by either a bolometer or crystal diode, the output of which is fed into a high gain amplifier. With the klystron fixed at the resonant frequency of the cavity, the magnetic field is slowly varied and simultaneously

Figure 1: Block Diagram of Apparatus



modulated at 80 cps. The detected and amplified signal may be viewed directly on an oscilloscope or channeled in a narrow band phase sensitive detector of standard design for pen recorder presentation of the derivative of the absorption curve.

The nitrogen afterglow is excited upstream by a microwave electrodeless discharge and pumped through the test cavity at a speed of approximately 0.5 liters per second by a Cenco Megavac pump. The discharge is excited by the strong electric fields in a 10 cm rectangular resonant cavity driven by a high powered QK-60 Raytheon magnetron.

MAGNET AND REGULATED POWER SUPPLY

The magnet is of the high impedance type similar to one originally developed at Stanford University. With a current of 2.8 amperes a maximum field of approximately 11,500 gauss is induced over a pole face 12" in diameter and a gap 2-3/4" in width.

The basis for the stability of the magnetic field is a regulatory circuit that maintains a constant voltage across a set of precision Dalohm resistors in series with the magnet coils. This voltage is compared to some fraction of the voltage from a set of Mallory mercury cells. The resulting d.c. error voltage, which is determined by the setting of a 100 K ohm Helipot variable resistor and the deviation of the magnet current from a fixed value, is amplified by a "chopper" type amplifier. The amplified d.c. voltage, applied as the grid potential of a set of eight 304 TL triodes, also in series with the magnet coils, controls directly the current flowing to the magnet. The magnetic field may be varied by changing the setting of the Helipot either manually or automatically with an electric clock motor.

The magnetic field, when measured with a nuclear induction apparatus was found to have a short time stability of approximately one part in one million. The inhomogeneity of the field was measured as approximately 5 parts in one million over a 2 cc volume.

THE RESONANT CAVITY

The TE_{011} cylindrical cavity mode is particularly useful for our experiments. The field configuration is indicated qualitatively in Figure 5 and is described analytically in terms of the usual cylindrical components, viz:¹⁷

$$E_r = E_z = H_\theta = 0,$$

$$E_\theta = J_0(3.832r/R) \sin(\pi z/L),$$

$$H_r = -k_z/k J_1(3.832r/R) \cos(\pi z/L),$$

$$H_z = k_1/k J_0(3.832r/R) \sin(\pi z/L),$$

where R and L are respectively the radius and the height of the cavity. The electric field is small near the axis of the cavity allowing the quartz flow tube to be inserted coaxially without appreciable dielectric loading. The cavity's Q is not greatly reduced by the holes drilled through its top and bottom since no radiofrequency currents need flow across these holes and since the power coupled out through the holes is reduced by brass sleeves dimensioned so the radiation is beyond "cutoff".¹⁸ The large radiofrequency magnetic fields along the cavity axis make possible high sensitivity for paramagnetic resonance in the flow section. In addition, as required for the observation of cyclotron

resonance, there is a component of the radiofrequency electric field perpendicular to the external magnetic field which is in the plane of a circular section of the cavity.

PROCEDURE

In carrying out the experimental observations the gas under study was injected into the flow system through a finely controllable needle valve. In the earliest experimentation with the nitrogen afterglow the relative percentage of oxygen "impurity" was adjusted to give the best resonance signal. However, in all of the nitrogen experiments reported here a near optimum fixed commercial mixture of 0.2 percent oxygen and 99.8 percent nitrogen was used in a fairly vacuum tight flow system, to avoid irreproducible electron densities. The pressure of the gas was measured with a Zimmerli manometer upstream from the discharge. The plate current of the exciting magnetron was held constant at an optimum value to eliminate the strength of the discharge as a source of variation in the electron production rate. While the quartz tube was carrying the afterglow from the discharge to the test cavity, the deflection of charged discharge products in the strong magnetic field was tending to keep noise producing ions from entering the cavity. Relatively low gas pressures were used since the production of electrons at pressures greater than about 10 mm of mercury became high enough to cause serious loading of the cavity. The low pressure limit was set by the disappearance of the afterglow and its associated electron density at about 1mm of mercury.

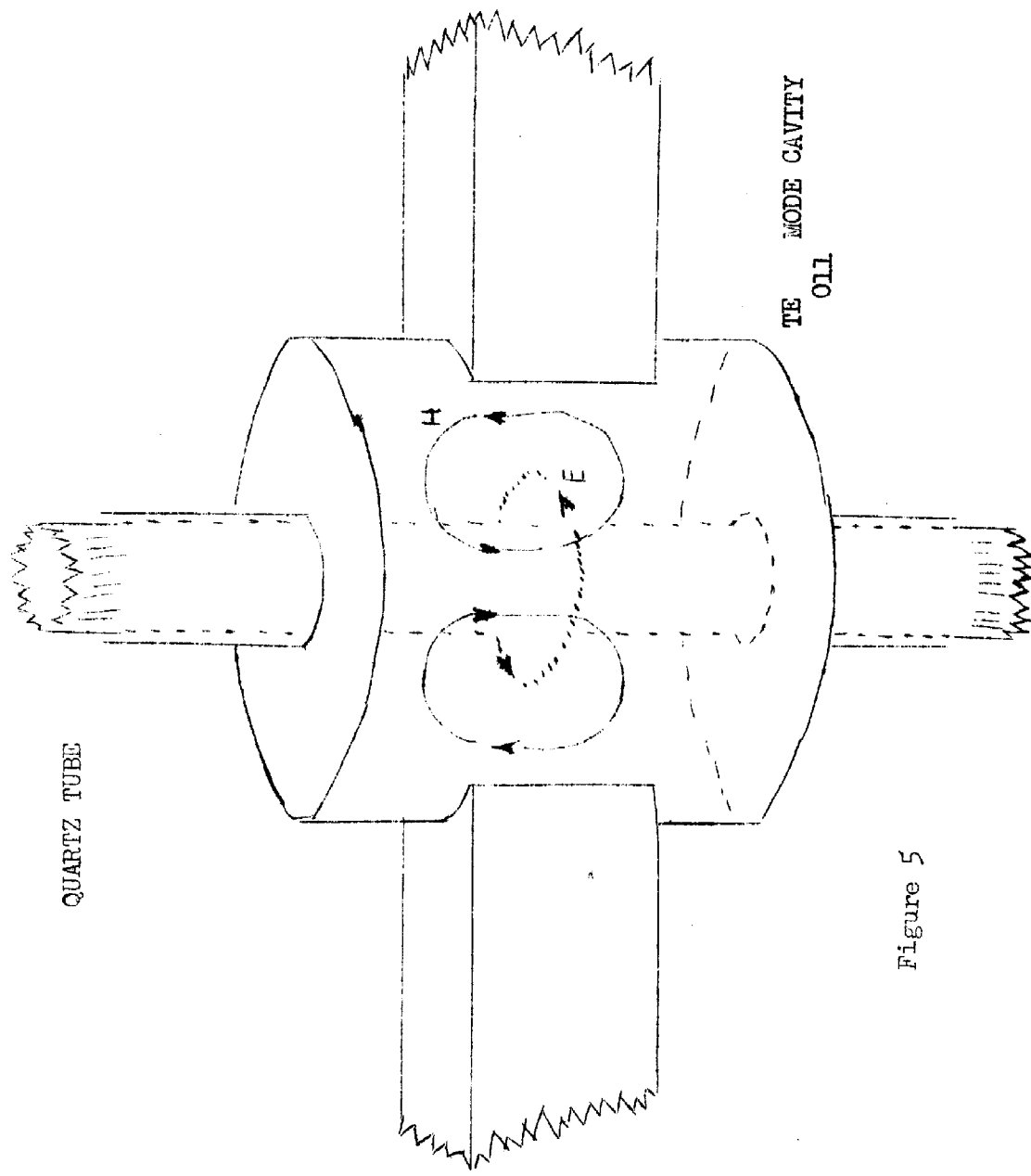


Figure 5

With the afterglow conditions held constant, the magnetic field was swept automatically through the resonant values to give recorder traces typified in Figure 6. The two narrow lines shown arise from the paramagnetic absorption of atomic oxygen and nitrogen, while the broad line arises from the cyclotron absorption of the electronic plasma broadened from the "heating" effects produced by the high powers necessary for observation of paramagnetic resonance. In measuring relative abundances, the paramagnetic species are viewed at the necessary high powers and then the microwave power should be reduced to levels where the line shape is less difficult to interpret. The bolometer detector was used at high power, but below one hundred microwatts, due to the rapid drop in bolometer sensitivity at low powers, a 1N23B crystal detector had to be used. An absolute calibration of the power transmitted to the detector at a specified level was made with a Hewlett-Packard bolometer bridge. Relative power levels were determined by the use of calibrated flap attenuators. The power dissipated in the cavity is inferred from the value of the power transmitted and a knowledge of relevant coupling factors. In the course of the experiments the incident radiofrequency power was varied by a factor of 10^4 .

C. THEORETICAL CONSIDERATIONS

NITROGEN AFTERGLOW

Before proceeding to an analysis of the cyclotron absorption process we shall briefly review the pertinent properties of the nitrogen afterglow. The glow that continues in nitrogen gas for an appreciable time after a discharge has passed through it, was reported as early as

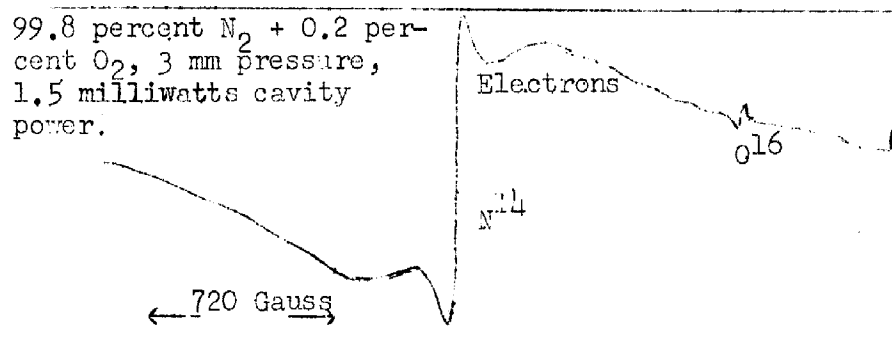


FIGURE 6: A recorder trace of the derivatives of the power absorption showing the simultaneous observation of cyclotron resonance and paramagnetic resonances of atomic nitrogen and oxygen. The broadening of the cyclotron resonance is due to the heating effect of the high r.f. level required for the observation of paramagnetic resonance.

1865 by Morren.¹⁹ Since then it has been rather extensively investigated by "classical" techniques.^{20,21,22} There now seems to be quite general agreement that the long living excitation energy of the glow's "active nitrogen" is stored in the dissociation of nitrogen molecules which recombine only in three body collisions in the body of the gas.* To keep the walls of the containing vessel from "sticking" nitrogen atoms and acting as a point of recombination, it is postulated that they are coated with a layer of, perhaps, nitrogen molecules which have a high reflection coefficient for incident nitrogen atoms. In terms of this picture, the emitted light of the afterglow, which is characteristic of the transition between the $B^3\Pi$ state and the metastable $A^3\Sigma$ state of the nitrogen molecule, may be explained as the simple recombination of two nitrogen atoms into an excited $B^3\Pi$ molecular state. On the other hand, this simple picture does not give a source for the ionization phenomena associated with the "active nitrogen". This difficulty was a point of considerable consternation for many years and led people to postulate other mechanisms for energy storage. However, recent work by Benson,⁹ involving microwave measurements of the associated electron densities, have established that the ionization is incidental rather than essential to the production of afterglows. Kunkel and Gardner,²³ also using static microwave techniques, have shown that the presence of nitric oxide is necessary for the production of electrons. In their experiments the loading effect i. e., the electron density of an afterglow flowing through a microwave cavity was measured as a function of the amount of oxygen or nitric oxide injected into the glow

* C. H. Reinecke, *Zeit. f. Physik*, 135, 36, (1953).

upstream from the test cavity. It was found that the addition of trace amounts of these gases increased the electron density tremendously (in fact 0.1 percent nitric oxide doubles the electron density). They proposed two mechanisms by which the energy of the active nitrogen may be converted into ionization energy, viz: direct ionization of nitric oxide in a triple collision with two nitrogen atoms or ionization of nitric oxide in a binary collision with a metastable nitrogen molecule which has been excited by a triple collision with nitrogen atoms. It is sufficient, for the purposes of the interpretation of our experiments, to assume that electrons are continuously generated in the body of the glowing column and that these electrons have energies such that predominantly elastic collisions are made with the nitrogen molecules. It might be noted at this point, apropos to the continuous generation hypothesis, that a diffusion calculation of the number of electrons capable of diffusing from the discharge into the test cavity in our experiments makes it inconceivable that the observed electrons could originate in the discharge.

THEORY

The goal of our theoretical analysis of the cyclotron resonance phenomenon is two-fold. Firstly, applying the simplest possible model of cyclotron power absorption, we can derive an expression relating the electron density to the observed line intensity. Secondly, we consider a more detailed theory which may enable us to infer from the experimental line shapes the dependence of the electronic collision cross section on pressure and effective temperature as determined by the incident radiation.

According to elementary theory, a free charged particle in motion in a static magnetic field H will execute circular orbits with a rotational frequency of $\omega_c = eH/mc$. When an electric field of frequency ω acts on this particle, the system will behave like a driven oscillator which resonates when ω approaches the "natural" frequency ω_c . According to Lorentz,²⁴ the particle's drift velocity should obey the equation of motion

$$m \left(\dot{\vec{v}} + \frac{1}{\tau} \vec{v} \right) = e \left(\vec{E} + \frac{\vec{v} \times \vec{H}}{c} \right), \quad (1)$$

where τ is the mean free time between collisions. This equation simply assumes that the mean momentum loss per collision is \vec{mv} . If the particle is driven in spiral orbits by a circularly polarized radiofrequency electric field $\vec{E} = [E_0/2 \sin \omega t, E_0/2 \cos \omega t, E_z(t)]$ and if H is parallel to the z -axis, the time dependence of the velocity is represented by $\vec{v} = [v_0(t) \sin(\omega t + \phi), v_0(t) \cos(\omega t + \phi), v_z(t)]$, where ϕ specifies the phase with respect to \vec{E} of a particular electron at "birth". $E_z(t)$ in our case is a periodic function but need not concern us since the v_z motion is not restricted by the magnetic field and does not contribute to the resonant process. The pertinent x - and y -components of equation (1) can be written in the complex form

$$\dot{u} + \frac{1}{\tau} u = -\frac{e}{m} \Sigma + i\omega_c u,$$

where $u = v_x + iv_y = v_0 e^{i\omega t + i\phi}$ and $\Sigma = E_x + iE_y = \frac{1}{2} E_0 e^{i\omega t}$. The solution for the complex drift velocity u is readily obtained as

$$u = \frac{e\Sigma}{m} [1 + i(\omega - \omega_c)] \tau \left[\frac{\tau}{1 + \tau^2(\omega_c - \omega)^2} \right].$$

The time average of the real power absorbed by an electron with mean free time τ is given as

$$(P_a)_\tau = \frac{1}{2} \mathbf{j} \cdot \mathbf{E} = \frac{1}{2} e u \Sigma = \frac{e^2 E_0^2 \tau}{4m} [1 + \tau^2(\omega_c - \omega)^2]^{-1} \quad (2)$$

In the actual experimental setup, the applied electric field can be considered as having a linear polarization in the x-direction and a time variation $E_0 \sin \omega t$ where E_0 is a spacially varying function. However, following the usual practice, the linearly polarized field can be resolved into two oppositely rotating circularly polarized fields each of amplitude $E_0/2$. From equation (2) it is seen that the sharply resonant, Lorentzian line shape is obtained from the component for which $\omega_c \cong \omega$, while the oppositely rotating component gives a broad absorption which is negligible in our experiments since $\omega\tau > 1$.

The total power absorbed would be found by integrating equation (2) over a suitable distribution of τ 's. In general, the heating of the system due to enhanced power absorption causes radical departures in the velocity distribution from the normally expected Boltzmann function. Later we shall try to account for these changes in terms of the more sophisticated diffusion theory. However, for the purposes of the abundance measurements at low power levels it is sufficient to assume that equation (2) multiplied by the total number of electrons gives the total power absorption, where τ now becomes the average mean free time.

In past studies of nuclear and electronic paramagnetic resonance, it has been found²⁵ that if the line width is determined predominantly by a relaxation process and not a magnetic inhomogeneity, the power absorbed by n_s paramagnetic species with magnetic moment $g\mu_B J$ can be represented to good approximation by a Lorentzian line shape of the form

$$P_a = \frac{n_s g^2 \mu_B^2 \omega^2 J(J+1) H_1^2}{12kT} \left[\frac{T_2}{1 + (\omega - \omega_0)^2 T_2^2} \right], \quad (3)$$

where ω is the frequency at which the resonance is observed and H_1 is the amplitude of the linearly polarized radiofrequency magnetic field. Unfortunately, the fact that we observe experimentally the derivative of the line intensity complicates things. Since the power level itself P_L is proportional to the total Q of the cavity Q_T , the recorded signal is related to the change in the total Q , ΔQ_T , by

$$S \propto \Delta P_L \propto P_L (\Delta Q_T / Q_T). \quad (4)$$

But Q_T is given by

$$\frac{1}{Q_T} = \frac{1}{Q_C} + \frac{1}{Q_S},$$

where Q_C is the loaded Q of the empty cavity and Q_S is the equivalent Q of the sample resonance. Since $Q_S \gg Q_C$

$$Q_T \cong Q_C (1 - Q_C / Q_S),$$

and (4) becomes

$$S \propto \Delta P_L \propto P_L \Delta(Q_C / Q_S).$$

Actually, the detected power is modulated by a sweep field of amplitude H_S , so

$$S \propto (\Delta P_C / \Delta H) H_S \propto H_S P_L \frac{d}{dH} (Q_C / Q_S).$$

In the usual formulation

$$Q = \frac{\text{Energy density}}{\text{Energy loss per radian}} = \frac{u}{\omega \int_V P_a dv},$$

where $\int_V P_a dv$ is the power absorption integrated over the volume of the cavity. Since neither Q_C nor u depend on the magnetic field,

$$S \propto H_S P_L \frac{d}{dH} \int_V P_a dv. \quad (4')$$

If we have paramagnetic gases at low pressures and electrons at low powers, we may assume that the lines shapes we will deal with in the density measurements can be expressed in a standardized Lorentzian form

$$P_a = \epsilon_a \left(\frac{\tau}{1 + \tau^2 \Delta^2} \right), \quad \Delta\omega = \omega - \omega_0,$$

then

$$S \propto H_S P_L \int_V \epsilon_a dv \left[\frac{d}{d\omega_0} \left(\frac{\tau}{1 + \tau^2 \Delta\omega^2} \right) \right].$$

We can express the peak-to-peak meter excursion, which occurs at the inflection point $(\Delta\omega)_i = 1/\sqrt{3} \tau$, as

$$S_m = (\text{constant}) H_S P_L \tau^2 \int_V \epsilon_a dv. \quad (5)$$

Thus, in comparing the number of electrons to the number of magnetic dipoles in the same cavity, we have the expression

$$\frac{\int_V n_c E_o^2 dv}{\int_V n_s H_1^2 dv} = \frac{g^2 \mu_B^2 \omega^2 J(J+1)m}{3e^2 (kT)} \left(\frac{S_{mc}}{S_{ms}}\right) \left(\frac{H_{Ss}}{H_{Sc}}\right) \left(\frac{P_{Ls}}{P_{Lc}}\right) \left(\frac{\Delta H_c}{\Delta H_s}\right)^2, \quad (6)$$

where the subscripts s and c denote respectively the spin and cyclotron resonance quantities. If the experimental conditions are the same in the two cases the ratio of the densities for identical signals is

$$n_s/n_c = 4 \times 10^{13},$$

where $J = 1/2$ and $g = 2$ have been assumed. We see that the cyclotron resonance is enormously more sensitive than the spin resonance. In fact, it is estimated that we should be able to detect as few as 100 electrons/cc with our apparatus.

Up to this point we have considered cyclotron resonance purely from a classical point of view. It would perhaps be beneficial to examine whether this approach is strictly valid. If one solves the Schrödinger equation for a free nonrelativistic electron in a magnetic field and includes the effects of the electronic spin, the energy levels are found to be $E_{n,m} = (2n + 1 + g_e m) \mu_B H$ where n specifies the orbital levels and m the spin's Zeeman levels (Figure 7). The applied electric field couples to the electric dipole moment of the electronic orbits to produce electric dipole transitions ($\Delta n = \pm 1, \Delta m = 0$) which leads to cyclotron absorptions. The radiofrequency magnetic field induces magnetic dipole transitions ($\Delta n = 0, \Delta m = \pm 1$). Dingle²⁶ has shown that the probability for a cyclotron transition is proportional to the effective electric dipole moment. Since this moment ($\simeq e(\text{average radius of orbits}) \simeq 5 \times 10^{-13}$) is much greater than the magnetic dipole moment

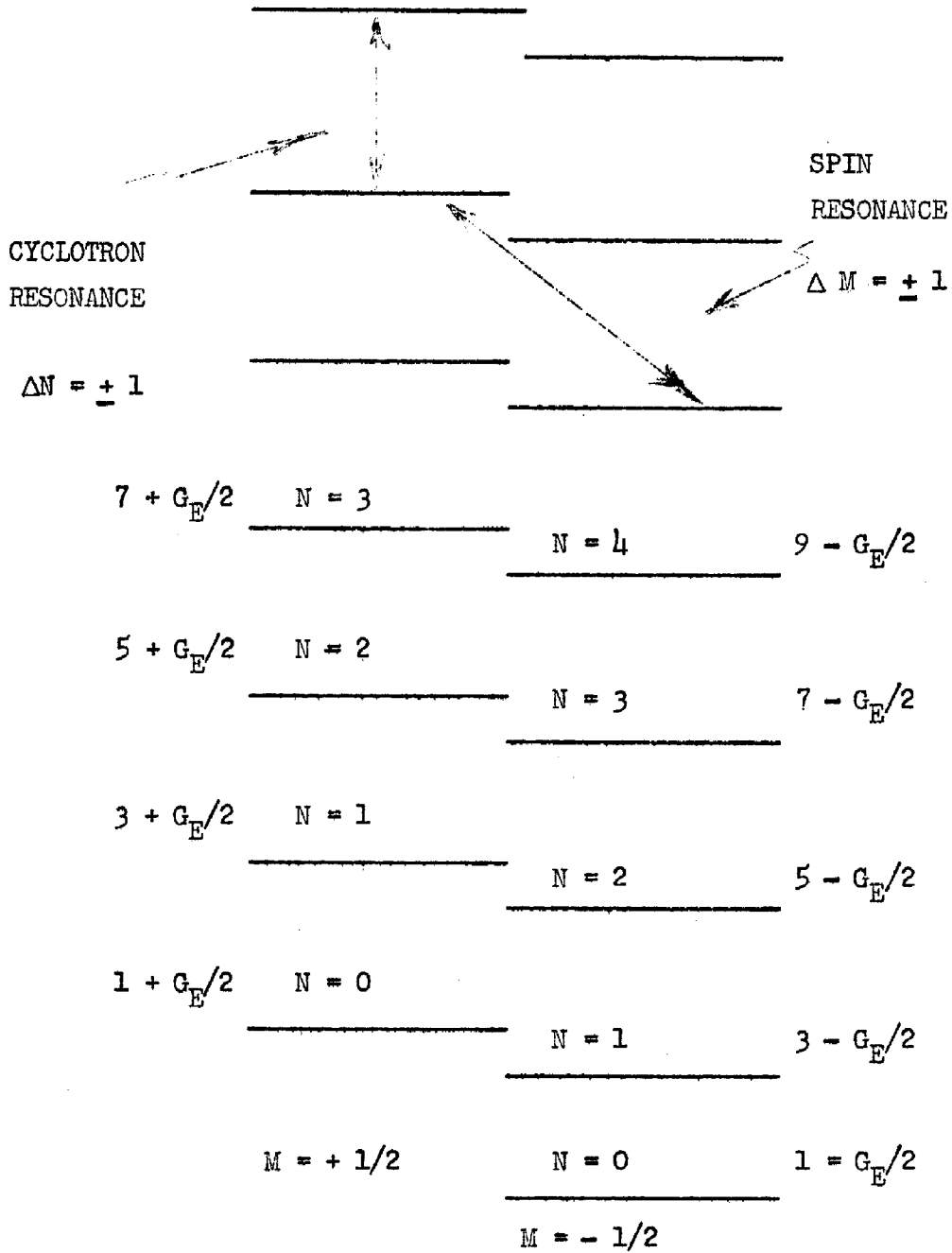


FIGURE 7 - ELECTRON ENERGY LEVELS:

$$E_{M,N} = \mu H(2N + 1 + M G_E)$$

($\approx \mu_B \approx 10^{-20}$) which determines the electronic spin flip transition probability, the orbital transition is about 5×10^7 times more probable than the spin flip. This higher probability can also be understood on the basis of the continuous nature of the orbital levels ($n = 0, 1, 2, \dots$). The electric field can excite a series of successive transitions limited only by its strength. In addition, all of the electrons contribute to the diamagnetic process, whereas only the statistical excess ($\approx \mu H/kT n$) is effective in the Zeeman case. Therefore, the possible spin resonance would be "lost" in the much stronger cyclotron transition, even though the two resonances occur at a slightly different frequency due to the fact that g_e is not exactly equal to two. These same reasons apply to explain the higher sensitivity of cyclotron resonance compared to all paramagnetic resonances.

The foregoing considerations are sufficient to enable one to measure abundances; however, we have carried the analysis one step further and applied the Boltzmann transport equation to the problem. The details of this work will be left to the Appendix and only the results will be summarized here. The Boltzmann theory takes into account the perturbations in the electronic velocity distribution imposed by external forces. The transport equation has the form

$$\left. \frac{\partial j(\underline{v}, \underline{r})}{\partial t} \right|_c = \frac{\partial j(\underline{v}, \underline{r})}{\partial t} + \underline{v} \cdot \nabla j(\underline{v}, \underline{r}) + \underline{a} \cdot \frac{\partial j(\underline{v}, \underline{r})}{\partial \underline{v}}, \quad (7)$$

where $j(\underline{v}, \underline{r}) d\underline{v} d\underline{r}$ is the number of electrons having respectively their velocities and positions in the range between $(\underline{v}, \underline{r})$ and $(\underline{v} + d\underline{v}, \underline{r} + d\underline{r})$,

\underline{a} is the externally imposed acceleration of the electrons, and $\left. \frac{\partial j}{\partial t} \right|_c$ is the change in $j(\underline{v}, \underline{r})$ due to collisions. It was assumed in solving equation (7) that the collisions are predominantly elastic, that $j(\underline{v}, \underline{r})$ is independent of spatial coordinates, and that the electrons are in dynamic - not thermal - equilibrium with the gas molecules. All of these assumptions are reasonable under our experimental conditions and in the low energy region (< 1 ev.) in which we are working. The resulting solution for $j(\underline{v})$ has been applied to find the power absorption by setting

$$P = \underline{j} \cdot \underline{E} = n_c e(\underline{v}) \cdot \underline{E} = n_c n_e E \cdot \int \underline{v} j(\underline{v}) d\underline{v} .$$

In order to carry out the solution for $j(\underline{v})$ some assumption about the dependence of the mean free path on velocity, $\lambda(v)$, must be made. $j(\underline{v})$ has been solved to first order in velocity with two separate assumptions about $\lambda(v)$. The simplest assumption of constant mean free time leads to a Lorentzian line shape independent of the heating effect of the incident power. This result is expected qualitatively since the assumption does not allow the electrons to warm up. The other, and perhaps most reasonable, simple assumption of constant mean free path leads to the much more complicated expression for the power absorption,

$$P_a = \frac{u_c e^2 E_o^2 \lambda}{6 \sqrt{2} (kT)^{1/2}} g(x_1, \alpha), \quad (8)$$

where

$$g(x_1, \alpha) = \frac{\int_0^\infty x^2 (x + x_1 + \alpha)^{\alpha-1} e^{-x} dx}{\int_0^\infty x^{1/2} (x + x_1 + \alpha)^\alpha e^{-x} dx} \quad (9)$$

is a dimensionless line shape function, $x_1 = \frac{1}{2} m\lambda^2(\Delta\omega)^2/kT$, and

$$\alpha = \frac{M}{6m} (eE_0\lambda/2kT)^2.$$

This parameter α can be given a physical interpretation. Since there is an equal a priori probability that a given electron has any phase ϕ with respect to the radiofrequency field, we may assume that the average energy gained per electron Σ_g in a mean free path is one-half the net energy gained by two electrons initially moving in the opposite directions. The electron out of phase will lose energy while the in-phase electron will gain energy. At exact resonance, $\omega = \omega_c$, an elementary calculation yields $\Sigma_g = \frac{1}{2} (e^2 E_c^2 r^2 / 4m)$. The energy loss per elastic collision Σ_L will be given by $(2m/M)(3kT_e/2)$, where M is the mass of the scattering molecules and T_e is the "effective" temperature of the electrons. Therefore α can be expressed as $3(T_e/T)^2 \cdot (\Sigma_g/\Sigma_L)$. At high power levels $\Sigma_g \simeq \Sigma_L$, so α is a measure of the square of the effective temperature in units of the gas temperature; while at low powers $T_e \simeq T$, so α now measures Σ_g/Σ_L . $g(x_1, \alpha)$ can be expressed as

$$g(x_1, \alpha) = \frac{4}{\sqrt{\pi}} (x_1 + \alpha)^{1/2} \frac{\Psi(3, \alpha + 3; x_1 + \alpha)}{\Psi(3/2, \alpha + 5/2; x_1 + \alpha)},$$

where the Ψ 's indicated are confluent hypergeometric functions of the second kind.²⁷ Unfortunately, these functions are not tabulated for usefully large values of α (average experimental values of α are of the order 10). Numerical evaluations of dg/dH have been performed for $\alpha = 0, 1, 2$. These curves are shown in Figure 8 and indicated analytically in the Appendix. An elementary approximation for $\alpha > 1$ [equation

is a dimensionless line shape function, $x_1 = \frac{1}{2} m\lambda^2(\Delta\omega)^2/kT$, and

$$\alpha = \frac{M}{6m} (eE_0\lambda/2kT)^2.$$

This parameter α can be given a physical interpretation. Since there is an equal a priori probability that a given electron has any phase ϕ with respect to the radiofrequency field, we may assume that the average energy gained per electron Σ_g in a mean free path is one-half the net energy gained by two electrons initially moving in the opposite directions. The electron out of phase will lose energy while the in-phase electron will gain energy. At exact resonance, $\omega = \omega_c$, an elementary calculation yields $\Sigma_g = \frac{1}{2} (e^2 E_c^2 r^2 / 4m)$. The energy loss per elastic collision Σ_L will be given by $(2m/M)(3kT_e/2)$, where M is the mass of the scattering molecules and T_e is the "effective" temperature of the electrons. Therefore α can be expressed as $3(T_e/T)^2 \cdot (\Sigma_g/\Sigma_L)$. At high power levels $\Sigma_g \simeq \Sigma_L$, so α is a measure of the square of the effective temperature in units of the gas temperature; while at low powers $T_e \simeq T$, so α now measures Σ_g/Σ_L . $g(x_1, \alpha)$ can be expressed as

$$g(x_1, \alpha) = \frac{4}{\sqrt{\pi}} (x_1 + \alpha)^{1/2} \frac{\Psi(3, \alpha + 3; x_1 + \alpha)}{\Psi(3/2, \alpha + 5/2; x_1 + \alpha)},$$

where the Ψ 's indicated are confluent hypergeometric functions of the second kind.²⁷ Unfortunately, these functions are not tabulated for usefully large values of α (average experimental values of α are of the order 10). Numerical evaluations of dg/dH have been performed for $\alpha = 0, 1, 2$. These curves are shown in Figure 8 and indicated analytically in the Appendix. An elementary approximation for $\alpha > 1$ [equation

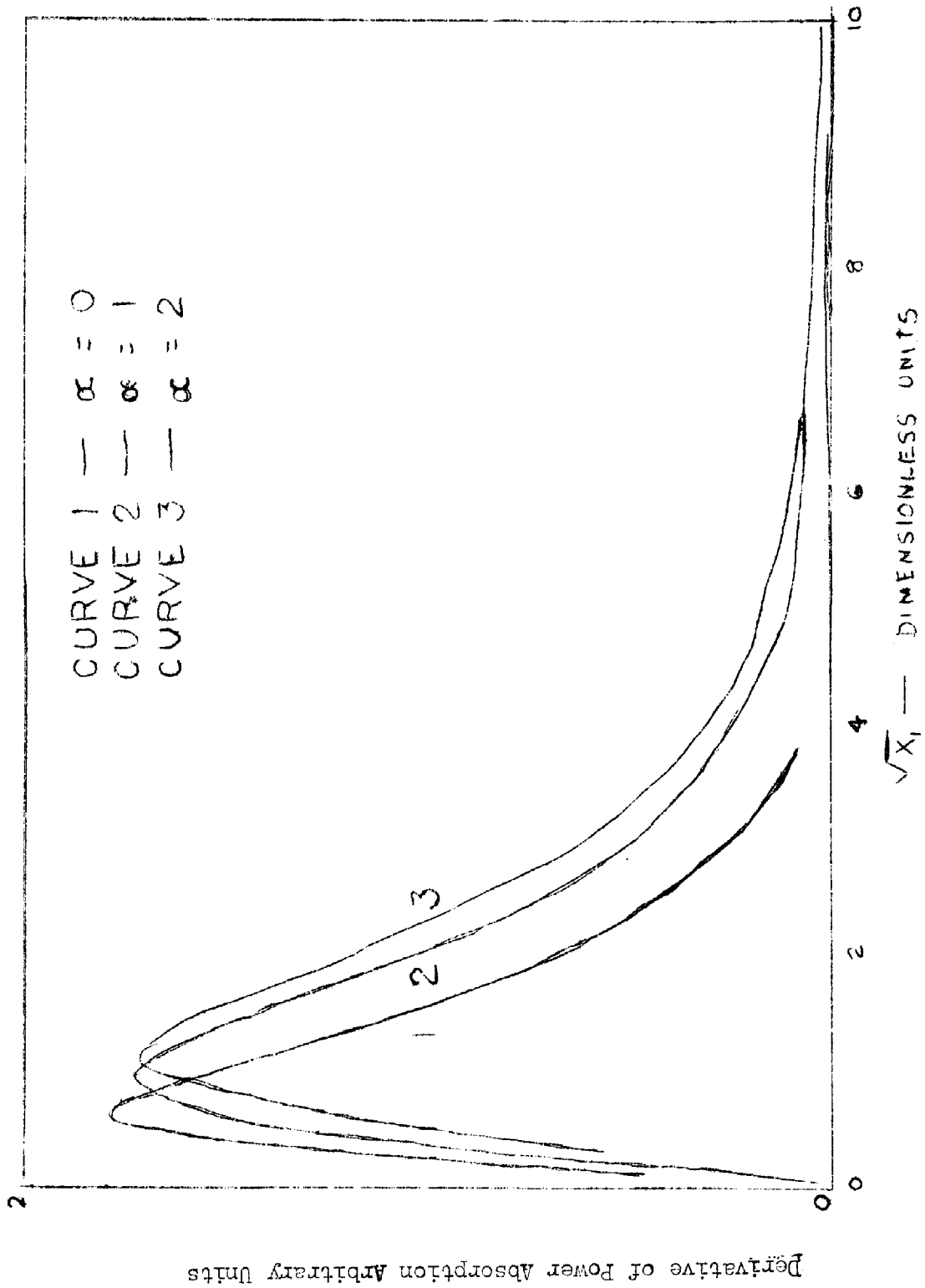


FIGURE 8 — THEORETICAL CURVES

(23) Appendix] is given by

$$g(x_1, \alpha) \propto e^{-\frac{x_1}{\sqrt{2\alpha}}(1 + x_1^2/16\alpha)}, \quad (10)$$

and

$$(x_1)_i \cong (x_1)_{1/2} \cong 0.92 \sqrt{\alpha}, \quad (11)$$

where $(x_1)_i$ and $(x_1)_{1/2}$ are respectively the values of x_1 at the inflection and half-maximum point of g . It is interesting to note that (11) leads to a line width proportional to $(E/\lambda)^{1/2}$ which is consistent with a result derivable from elementary considerations at high powers. The limiting heating, within the assumption of elastic collisions, is obtained, as mentioned above, when the energy gained by the system in a mean free path is lost in the concluding collision with a molecule of mass M . Expressing Σ_1 as $(2m/M)(\frac{1}{2} \bar{m} \bar{v}^2) = m^2 \lambda^2 / M \tau^2$, where \bar{v} is the average velocity of the electrons, and setting $\Sigma_g = \Sigma_e$, we obtain simply that

$$1/\tau = 0.707(M/2m)^{1/4} (eE_0/m\lambda)^{1/2},$$

which compares remarkably well with

$$(\Delta\omega)_{1/2} \cong 0.745(M/2m)^{1/4} (eE_0/m\lambda)^{1/2},$$

from equation (11). The low power results ($\alpha \leq 1$) indicate a line width independent of power, as expected. The expression for the mean free path obtained from the curve for $\alpha = 0$ (Figure 8),

$$\lambda = 0.373 \frac{1}{(\Delta H)_i} \text{ cm}, \quad (12)$$

is consistent with the similar expression

$$\lambda = 0.437 \frac{1}{(\Delta H)_i} \text{ cm}, \quad (13)$$

derivable from simple Lorentzian theory.

Because of the intractable nature of the integrals involved, solutions with other assumptions for $\lambda(v)$ have not been carried out. It would appear that the theoretical limit to the application of simple diffusion theory is imposed by the increasing effectiveness of inelastic collisions as one proceeds to high power levels. The point at which inelastic collisions become important experimentally can be estimated in the following manner: The ratio of the effective temperature of the heated electrons to that of unheated electrons will be proportional to the ratio of the squares of the average velocities in the two cases - i.e.,

$$T_e/T = v^2/v_0^2 = \frac{\lambda^2/\tau^2}{\lambda_0^2/\tau_0^2}.$$

If we again assume that λ is relatively independent of velocity, then

$$T_e/T \simeq \Delta H^2/\Delta H_0^2,$$

where ΔH and ΔH_0 represent respectively the experimental line widths at finite and vanishing power levels. If we assume that the onset of appreciable inelastic processes is determined by the excitation of the first electron level of the nitrogen molecule at 6 ev ($A^3 \Sigma$), then there will be sufficient spread in the energy distribution at $3kT_e/2 \simeq 4$ ev to excite these levels. Therefore, if $\Delta H \simeq 10 \Delta H_0$ ($3kT_e/2 \simeq 0.04$ ev), we should expect deviations from theories derived by an elastic assumption.

D. EXPERIMENTAL RESULTS

ABUNDANCE MEASUREMENTS

Since neither an extensive nor a systematic series of abundance measurements under a variety of conditions were contemplated or carried out, only typical observed densities will be reported here. To calibrate the absolute sensitivity of the apparatus for paramagnetic resonance, a small capillary, containing 10^{16} Mn^{2+} ions in solution, was placed along the axis of the test cavity and the signal intensity of one of the six hyperfine components - *i. e.*, $1/6 \times 10^{16}$ spins - was recorded at a detector power level of 7 milliwatts. The average line width of these lines was about 40 gauss. After this calibration was made, then equation (6) was used to establish relative abundances.

In a nitrogen afterglow at a measured nitrogen pressure of 6 mm's of mercury with a 0.2 percent impurity of oxygen, one 0.5 gauss hyperfine component of the N^{14} resonance had a signal height of 2 relative to one of the calibrating Mn^{2+} hyperfine components, when observed at a detector power level of 2.7 milliwatts. Using these experimental values, we find an approximate density of

$$N(\text{N}) \cong 4.2 \times 10^{13} \text{ nitrogen atoms/cc,}$$

- *i. e.*, the gas was 0.02 percent "active". Under these same conditions, the signal height of the atomic oxygen resonance ($J = 2$, $g = 3/2$) was 1/12 that of atomic nitrogen. Hence, an atomic oxygen density

$$n(\text{O}) \cong 3.9 \times 10^{12} \text{ oxygen atoms/cc.}$$

The small number of oxygen molecules present ($\cong 4 \times 10^{14}$ per cc) have

a higher (1 percent) activation than the nitrogen molecules (0.02 percent), as one would expect from the lower dissociation energy of oxygen.

The chief difficulty in making good relative electron abundance determinations lies in the estimation of the integrals $\int n_c \bar{E}^2 dv$ and $\int n_s H^2 dv$. By considering the analytic expressions for the electric field configuration given in an earlier section we have estimated that the average electric field over the volume of the flow tube is 0.04 times the maximum value. Using this estimate equation (6) can be rewritten

$$\frac{n_c v_c}{(n_s v_s)_{Mn^{2+}}} = 3.3 \times 10^{-12} \left(\frac{H_{Ss}}{H_{Sc}}\right) \left(\frac{\Delta H_c}{\Delta H_s}\right)^2 \left(\frac{P_{Ls}}{P_{Lc}}\right)^2 \left(\frac{S_{mc}}{S_{ms}}\right), \quad (6')$$

where the extra factor (P_{Ls}/P_{Lc}) has come from the fact that $\bar{E}^2 = \bar{H}^2 \propto P_L$. At a measured pressure of 5mm's, the relative signal height of the 292 gauss cyclotron line is 27.6 with respect to the calibrating Mn^{2+} line, when the detector power level was 0.38 milliwatts. The density thus obtained is

$$n(e) = 8.4 \times 10^9 \text{ electrons/cc.}$$

A sharp experimental low power cyclotron resonance is shown in Figure 9 and is to be compared to the broad high power curve in Figure 6.

Careful searches were made for the paramagnetic resonances of the 2D and 2P metastable states of atomic nitrogen, molecular nitrogen oxide and peroxide. The negative results of these investigations indicate the following maximum densities for these species:

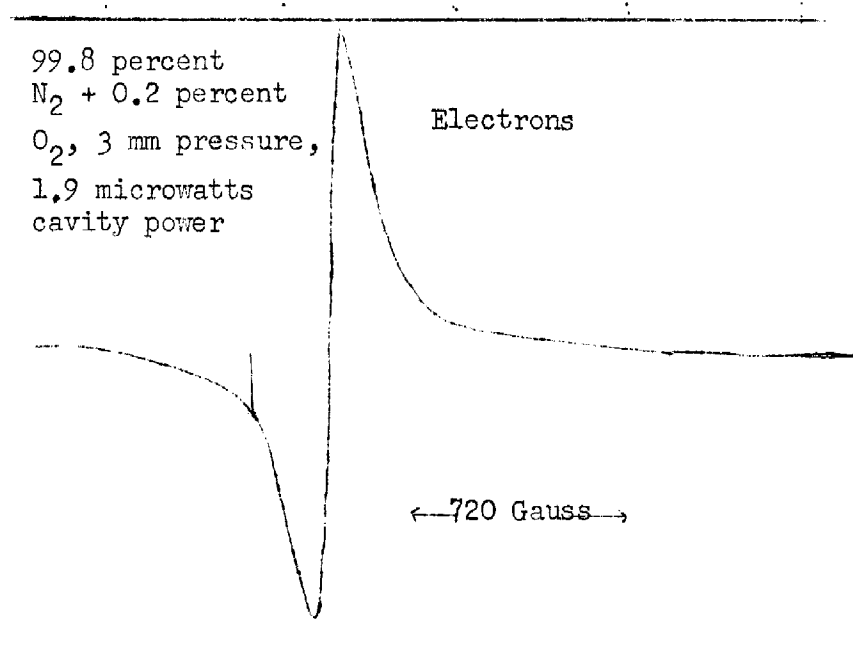


FIGURE 9: Derivative of a sharp cyclotron resonance absorption line obtained at low r.f. level (1.9 microwatts at the detector).

$$n(^2D \text{ or } ^2P \text{ N}) < 10^{12} \text{ atoms/cc,}$$

$$n(\text{NO or NO}_2) < 10^{13} \text{ molecules/cc.}$$

However, the real power of the cyclotron technique was revealed when the never-before-observed electrons in the pale green air afterglow - i.e., 20 percent oxygen and 80 percent nitrogen - gave excellent signals. Because of the low abundance of active nitrogen no atomic signals were observed, so

$$n(\text{N}) < 10^{12} \text{ nitrogen atoms/cc.}$$

However, the expected enhancement of the atomic oxygen signal was observed. The air afterglow at 4 mm had an approximate electron density

$$n(e) \cong 10^5 \text{ electrons/cc.}$$

The mechanism for the generation of these electrons is not established. It may be that a small trace of active nitrogen, not "used up" in dissociating oxygen, would be sufficient to maintain this electron density. It is interesting to note that, in contrast to the "pure" nitrogen case, the electron signal intensities in the air afterglow decrease with pressure and disappear at 7 mm. This curious behavior can perhaps be understood on the basis of the abnormally high electronic attachment coefficient of oxygen; as the pressure increases the probability that an electron will be captured and removed from the plasma before absorbing an appreciable amount of energy will also increase.

COLLISION CROSS SECTIONS

One of the difficulties encountered in carrying out a systematic study of the experimental line width as a function of incident power and

pressure was the presence of a background impurity paramagnetic signal at $g = 2.0$. This extremely sharp resonance ($\Delta H_i < 0.5$ gauss) which seems to be produced in the walls of the quartz flow tube by the action of the afterglow, can be eliminated by heating the tubing to between 600° to 800°C . However, the spurious signal returns within a short period of subsequent exposure to the afterglow. The annoying aspect of this impurity lies in the fact that it does not appear at very low powers, where cyclotron resonance is simple, because of the reduced sensitivity for paramagnetic resonance; while it is saturated out at high powers, where cyclotron resonance is complicated by inelastic collisions, because of its long relaxation time. It appears only in the 10 to 100 microwatt range of detector powers (α of the order 10) where the interesting things are happening in the simple cyclotron theory. The sharp impurity line, which produces a distortion in the experimental cyclotron curves, seems to be due to the paramagnetic behavior of some type of vacancy generated in the quartz by either the active nitrogen, electrons, or radiation from the discharge. It was also difficult to avoid distorted line shapes at low power levels, since the klystron frequency cannot be closely monitored for exact tuning.

However, the relatively reliable data obtained for nitrogen afterglows at pressures of 2, 3, 4, and 5 mm's of mercury and powers from 2 microwatts to 8 milliwatts and for an air afterglow at 2 mm's of mercury are plotted in Figure 12. The data at high levels seems generally to obey the expected $\Delta H \propto P^{1/4}$ relationship. Curves of $\Delta H \propto (E/\lambda)^{1/2}$ are plotted also for comparison. The horizontal axis

represents the measured power level at the detector, which is 0.195 times the power dissipated in the cavity. The deviation of some of the data from simple behavior may perhaps be to some extent explained by inelastic collisions. For example, some of the values of ΔH for pressures of 2 and 3 mm have increased by a factor of approximately ten from their low power values and hence from an argument in an earlier section we might expect elastic processes to be important.

Combining equations (12) and (13) with the experimental power limits for ΔH_i , calculations of λ and normalized collision probabilities $P_c = (\lambda p_{\text{mm}})^{-1}$, where p_{mm} is the pressure in millimeters of mercury, have been made and are tabulated in Table I. In this table the subscripts D and L denote respectively diffusion theory and simple Lorentzian theory quantities.

Table I

P_{mm}	H_i gauss	D cm	L cm	$(P_c)_D$ (cm - mm of Hg) ⁻¹	$(P_c)_L$ (cm - mm of Hg) ⁻¹
5	170	2.19×10^{-3}	2.57×10^{-3}	91.5	77.8
4	100	3.73	4.37	67.0	57.2
3	42	8.88	10.4	37.5	32.0
2	17	21.9	25.7	22.8	19.5

E. CONCLUSIONS

There seems to be no doubt that cyclotron resonance can be used, to sensitively detect and, under suitable conditions, to measure the densities of charge carriers in a plasma. The values obtained in our experiments

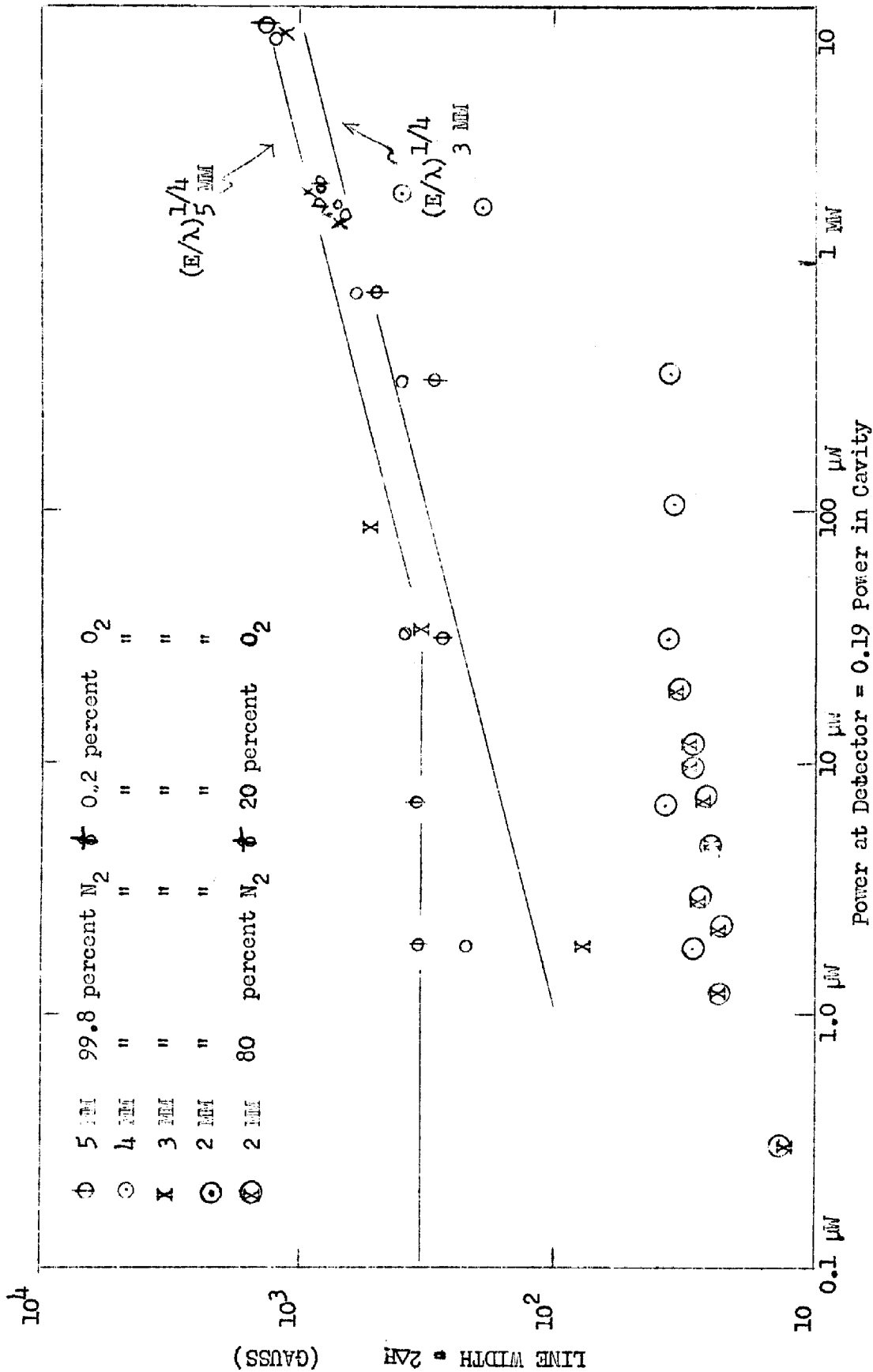


Figure 12 - Experiment Line Widths Vs R. F. Power

compare favorably with densities of approximately 10^8 electrons/cc deduced from less sensitive microwave conductivity measurements.^{9,23} Because of differences in flow rates, methods of excitations, and pressures it is difficult to make an exact comparison between these values. The technique could perhaps be fruitfully applied at lower radiofrequencies to measurements of heavier ion densities.

To understand the line shape theory, molecular nitrogen is rather an unfortunate place to start since the collision properties of molecular gases have anomalous features among which are the apparently very large energy losses in elastic collisions - i.e., each elastic collision seems to take up at least 20 times the expected $2m/M$ fraction of the average value of the electron's energy.²⁸ The values of P_c obtained seem to be at variance with the previously determined value $15 \text{ (cm - mm of Hg)}^{-1}$ for 0.039 ev electrons in molecular nitrogen.¹⁰

If suitable companion computational facilities for calculation of the diffusion integrals were available, it would seem worthwhile studying the afterglow electrons with simpler noble gas atoms as the main collision centers - i.e., just enough nitrogen would be added to, say, helium gas to maintain a continuous electron production. This suggestion points up some of the limitations of our simple technique, since its convenience rests on the rather unique nature of the nitrogen afterglow.

This research has been supported in part by the Research Corporation and the U. S. Atomic Energy Commission.

F. APPENDIX

DIFFUSION THEORY CALCULATION OF POWER ABSORPTION

Our treatment of the Boltzmann transport equation,

$$\left. \frac{\partial j}{\partial t} \right|_c = \frac{\partial j}{\partial t} + \underline{v} \cdot \underline{\Delta} j + \underline{a} \cdot \frac{\partial j}{\partial \underline{v}}, \quad (7)$$

generally follows that applied by Marganau²⁹ to the problem of non-resonant microwave electron conductivity. In our case

$$\underline{a} = \frac{e}{m} \underline{E} + \frac{e}{mc} \underline{v} \times \underline{H}.$$

We shall assume, as discussed in the text, that we have a circularly polarized electric field in the xy-plane and a magnetic field in the z-direction. So

$$\underline{a} = (\gamma \cos \omega t + \omega_c v_y) \underline{i} + (\gamma \sin \omega t - \omega_c v_x) \underline{j},$$

where $\gamma = eE_0/2m$ and $\omega_c = eH/mc$. The solutions of (7) can be expressed in terms of the spherical harmonics of the velocity. It is sufficient for our purposes to keep only terms of first order, so

$$j(\underline{v}) = j_0(v) + v_x [j_1(v) \cos \omega t + g_1(v) \sin \omega t] \\ + v_y [j_2(v) \cos \omega t + g_2(v) \sin \omega t]. \quad (14)$$

From kinetic theory³⁰ it is found that the discontinuous change in $j(\underline{v})$ due to elastic collisions is expressible as

$$\left. \frac{\partial j_0}{\partial t} \right|_{ec} = \frac{1}{v^2} \frac{m}{M} \frac{\partial}{\partial v} \left[\frac{v^4 j_0}{\lambda} \right] + \frac{KT}{Mv^2} \frac{\partial}{\partial v} \left[\frac{v^3}{\lambda} \frac{\partial j_0}{\partial v} \right] \quad (15)$$

$$\left. \frac{\partial F}{\partial t} \right|_{ec} = -\frac{v}{\lambda} F, \quad (16)$$

where $F = v_x j_1, v_y j_2, v_x g_1, v_y g_2$. The second term in (15) is small but necessary if j_0 is to approach a Boltzmann distribution as the electrons approach thermal equilibrium. If we assume that j is independent of spacial coordinates, then (7) becomes

$$\begin{aligned} \left. \frac{\partial j}{\partial v} \right|_{ec} &= \frac{v}{\lambda} [(j_0 \cos \omega t + g_1 \sin \omega t)v_x + (j_2 \cos \omega t + g_2 \sin \omega t)v_y] \\ &+ \omega [(g_1 \cos \omega t - j_1 \sin \omega t)v_x + (g_2 \cos \omega t - j_2 \sin \omega t)v_y] \\ &+ \omega_c [(g_1 \sin \omega t + j_1 \cos \omega t)v_y - (g_2 \sin \omega t + j_2 \cos \omega t)v_x] \\ &+ \gamma [\cos \omega t (\frac{v_x}{v} K + j_1 \cos \omega t + g_1 \sin \omega t) \\ &- \sin \omega t (\frac{v_y}{v} K + j_2 \cos \omega t + g_2 \sin \omega t)], \end{aligned} \quad (17)$$

where

$$K = \frac{\partial j_0}{\partial v} + v_x \left(\frac{\partial j_1}{\partial v} \cos \omega t + \frac{\partial g_1}{\partial v} \sin \omega t \right) + v_y \left(\frac{\partial j_2}{\partial v} \cos \omega t + \frac{\partial g_2}{\partial v} \sin \omega t \right).$$

Equating coefficients of respectively $v_x \sin \omega t$, $v_x \cos \omega t$, $v_y \sin \omega t$, $v_y \cos \omega t$, and the time average of their products, five independent linear equations are obtained which can be solved for j_1 , j_2 , g_1 , g_2 , and j_0 . We find

$$\begin{aligned} j_1 = g_2 &= -\gamma \lambda [v^2 + \lambda^2 (\omega_c + \omega)^2]^{-1} \frac{\partial j_0}{\partial v}, \\ j_2 = -g_1 &= \frac{\gamma \lambda^2}{v} [v^2 + \lambda^2 (\omega_c + \omega)^2]^{-1} \frac{\partial j_0}{\partial v}, \end{aligned}$$

$$j_0 = - \left\{ 1 + \frac{\gamma^2 \lambda^2 M}{3kT} [v^2 + \lambda^2 (\omega_c + \omega)^2]^{-1} \right\} \frac{\partial j_0}{\partial v}$$

The power absorption then will be found from

$$\begin{aligned} P_a &= \underline{j} \cdot \underline{E} = e(\bar{v}_x E_x + \bar{v}_y E_y) \\ &= m\gamma [\cos \omega t \int_{\underline{v}} v_x j(\underline{v}) d\underline{v} + \sin \omega t \int_{\underline{v}} v_y j(\underline{v}) d\underline{v}] \end{aligned}$$

When the time average of P_a is carried out

$$\begin{aligned} P_a &= \frac{m\gamma}{2} \left[\int_{\underline{v}} v_x^2 j_1(\underline{v}) d\underline{v} + \int_{\underline{v}} v_y^2 j_1(\underline{v}) d\underline{v} \right] \\ &= \frac{m\gamma}{3} \int_{\underline{v}} v^2 j_1(\underline{v}) d\underline{v} \\ &= \frac{4\pi m\gamma}{3} \int v^4 j_1(\underline{v}) d\underline{v}. \end{aligned} \quad (18)$$

The equations that must be solved with some assumption about $\lambda(v)$ are

$$\frac{\partial j_0}{\partial x} = - \left(\frac{x + x_1}{x + x_1 + a} \right) j_0, \quad (19)$$

and

$$j_1 = \frac{\gamma \lambda m}{2kT} \left(\frac{mv}{KT} \right) (x + x_1 + a)^{-1} j_0, \quad (20)$$

where

$$x = \frac{1}{2} mv^2/kT.$$

1. Constant mean free time assumption In this case equation (19)

becomes

$$\partial j_0 / \partial x = - (T/T_c) j_0,$$

or

$$j_0 = A e^{-(T/T_c)x},$$

where

$$T_e = T \left[1 + \frac{\gamma^2 M \tau^2}{3kT} \left(\frac{1}{1 + \tau^2 \Delta \omega^2} \right) \right],$$

and A is a constant of integration determined from $n = \int j(v) dv$.

Therefore

$$\begin{aligned} P_a &= \frac{2\gamma^2 v_m}{3} \left(\frac{1}{1 + \tau^2 \Delta \omega^2} \right) \frac{\int_0^\infty u^{3/2} e^{-u} du}{\int_0^\infty u^{1/2} e^{-u} du} \\ &= \frac{e^2 E_0^2 \tau}{4m} \left(\frac{1}{1 + \tau^2 \Delta \omega^2} \right), \end{aligned} \quad (21)$$

which is independent of the power level. However, in determining the mean free path from experimental line widths, one would use an average velocity $\bar{v} = (3kT_e/m)^{1/2}$.

2. Constant mean free path assumption: For $\lambda = \text{constant}$, equation (19) integrates immediately to give

$$j_0 = A \left(\frac{x_1 + \alpha + x}{x_1 + \alpha} \right)^\alpha e^{-x}, \quad (22)$$

and

$$j_1 = \frac{\gamma \lambda m}{2kT(x_1 + \alpha)} \left(\frac{mv}{kT} \right) \left(\frac{x_1 + x + \alpha}{x_1 + \alpha} \right)^{\alpha-1} e^{-x},$$

which in turn leads to

$$P_a = \frac{\frac{1}{2} \gamma^2 \lambda}{3} \left(\frac{2m^3}{kT} \right)^{1/2} \frac{\int_0^\infty x^2 (x_1 + \alpha + x)^\alpha e^{-x} dx}{\int_0^\infty x^{1/2} (x_1 + \alpha + x)^\alpha e^{-x} dx}$$

or

$$P_a = \frac{ne^2 E_0^2 \lambda}{6\sqrt{2} (mkT)^{1/2}} g(\alpha, x_1), \quad (23)$$

where

$$g(\alpha, x_1) = \frac{\int_0^{\infty} x^2 (x_1 + \alpha + x)^{\alpha-1} e^{-x} dx}{\int_0^{\infty} x^{1/2} (x_1 + \alpha + x)^{\alpha} e^{-x} dx}$$

As pointed out in the text, g can be expressed in terms of solutions of the confluent hypergeometric equation.

A simple approximation can be made if g is written

$$g(\alpha, x_1) = \frac{\int_0^{\infty} F_1(\alpha, x, x_1) dx}{\int_0^{\infty} F_2(\alpha, x, x_1) dx},$$

and if it is noted that both $F_1 = x^2(x + x_1 + \alpha)^{\alpha-1} e^{-x}$ and $F_2 = x^{1/2}(x + x_1 + \alpha)^{\alpha} e^{-x}$ are sharply peaked around their maximum values $F(x_m)$, since then the line shape can be expressed as

$$g \propto \frac{F_1(x_m) \cdot \Delta x_1}{F_2(x_m) \cdot \Delta x_2}, \quad (24)$$

where the Δx 's correspond to half widths of the F 's. In fact, because of the general similarity of the F 's, to first approximation (24) reduces to

$$g \propto \frac{F_1(x_m)}{F_2(x_m)}. \quad (25)$$

By setting the second derivatives of the F 's equal to zero and assuming $\sqrt{\alpha} > 1$, we obtain the following estimates of the x_m 's:

$$(x_m)_1 = [2(x_1 + \alpha)]^{1/2} \left[1 + \frac{(x_1 - 1)^2 - 4(x_1 - 1)[2(x_1 + \alpha)]^{1/2}}{16(x_1 + \alpha)} \right],$$

$$(x_m)_2 = \left(\frac{x_1 + \alpha}{2} \right)^{1/2} \left[1 + \frac{(x_1 - 1/2)^2 - 2(x_1 - 1/2)[2(x_1 + \alpha)]^{1/2}}{4(x_1 + \alpha)} \right].$$

These estimates in turn lead to an approximate line shape function

$$g(x_1, \alpha) \propto e^{-\frac{x_1}{\sqrt{2\alpha}}(1 + x_1^2/16\alpha)} \quad (26)$$

The solution of the simple cubic equation for the half-width-at-half-maximum of (26) is given by

$$(x_1)_{1/2} \approx 0.92 \sqrt{\alpha} .$$

This value also approximates numerically the inflection point $(x_1)_i$ of (26).

The algebraic expansion of equation (21) leads to the following values for dg/dH at $\alpha = 0, 1,$ and 2 :

$$\left. \frac{dg}{dH} \right|_{\alpha=0} \propto \sqrt{x_1} [x_1(2 + x_1)e^{x_1}] [-E_1(-x_1) - (L + x_1)],$$

$$\left. \frac{dg}{dH} \right|_{\alpha=1} \propto \sqrt{x_1} (2x_1 + 5)^{-2} ,$$

$$\left. \frac{dg}{dH} \right|_{\alpha=2} \propto \sqrt{x_1} \frac{4x_1^2 + 24x_1 + 21}{(4x_1^2 + 12x_1 + 15)^2} .$$

These functions are normalized and plotted in Figure 8.

REFERENCES

1. G. Dresselhaus, A. F. Kip, and C. Kittel, Phys. Rev. 98, 368 (1955).
2. B. Lax, H. J. Zeiger, R. N. Dexter, and E. S. Rosenblum, Phys. Rev. 93, 1418 (1954); R. N. Dexter, H. J. Zeiger, and B. Lax, Phys. Rev. 95, 557 (1954).
3. D. J. E. Ingram and J. G. Tapley, Phys. Rev. 97, 238 (1955).
4. B. Lax, W. P. Allis, and S. C. Brown, Jour. App. Phys. 21, 238 (1950).
5. L. Goldstein, M. Lampert, and J. Henry, Phys. Rev. 82, 956 (1951); L. Goldstein, M. Lampert, and J. Henry, Phys. Rev. 83, 755 (1951).
6. L. Goldstein, private communication.
7. P. Franken, private communication.
8. R. Beringer, private communication.
9. J. H. Benson, Jour. App. Phys. 23, 757 (1952).
10. A. V. Phelps, O. I. Fundingsland, and S. C. Brown, Phys. Rev. 84, 559 (1951).
11. R. Beringer and J. G. Castle, Phys. Rev. 78, 581 (1950); R. Beringer, E. B. Rawson, and A. F. Henry, Phys. Rev. 94, 343 (1954).
12. R. Beringer and J. G. Castle, Phys. Rev. 80, 114 (1950).
13. R. Beringer and M. A. Heald, Phys. Rev. 95, 1474 (1950).
14. M. A. Heald and R. Beringer, Phys. Rev. 96, 645 (1954).
15. R. Beringer and J. G. Castle, Phys. Rev. 81, 82 (1954).
16. E. B. Rawson and R. Beringer, Phys. Rev. 88, 677 (1952).
17. R. Beringer, M. I. T. Radiation Laboratory Series, vol. 11, pp. 299.
18. E. B. Rawson, Thesis, Yale University, 1952; see also reference 13.
19. Morren, Annales de Chimie et de Physique, Series 4, 4, 293 (1865).
20. E. D. Lewis, Astrophysical Jour. 12, 8 (1900).
21. Rayleigh, Proc. Roy. Soc. 151A, 567 (1935); Rayleigh, Proc. Roy. Soc. 180A, 123 (1942).

22. S. K. Mitra, Active Nitrogen - A New Theory, India Press, Ltd., Calcutta (1945); S. K. Mitra, Phys. Rev. 90, 516 (1953).
23. A. Gardner, Tech. Report HE-150-129, Institute of Engineering Research, University of California, Bull. Am. Phys. Soc. 29, No. 8, p. 15 (1954).
24. H. A. Lorentz, The Theory of Electrons, G. E. Stechert, New York (1916).
25. N. Bloembergen, E. M. Purcell, R. V. Pound, Phys. Rev. 73, 679 (1948).
26. R. B. Dingle, Proc. Roy. Soc. 212A, 38 (1952).
27. Erdelyi, Magnus, Oberheltinger, Tuiomi, Higher Transcendental Functions, vol. I, p. 255, McGraw-Hill Book Company, Inc. (1953).
28. Massey and Burhop, Electronic and Ionic Impact Phenomena, p. 279, Oxford Clarendon Press (1952).
29. H. Margenau, Phys. Rev. 69, 508 (1946).
30. Chapman and Cowling, Mathematical Theory of Non-Uniform Gases, p. 348, Cambridge University Press, New York (1939).